Research article

Investigation of delivery mechanism of curcumin loaded in a core of zein with a double-layer shell of chitosan and alginate

Amitis Aghelinejad , Nadereh Golshan Ebrahimi *

Polymer Engineering Department, Chemical Engineering Faculty, Tarbiat Modares University, Tehran, Iran

A B S T R A C T

The pursuit of efficient drug delivery systems has led to innovative approaches such as matrix and core-shell structures. This study explores these systems with a focus on enhancing the delivery and stability of curcumin, a bioactive compound with therapeutic potential. Matrix systems using zein protein were fabricated through coaxial airflow extrusion with a vibration generator, while core-shell systems were produced using concentric nozzles. Double-layer reservoir systems were also formed by coating chitosan-shelled structures with an alginate solution. Encapsulation of curcumin within each system was confirmed through FTIR and optical microscope analysis, followed by efficiency evaluation, which was measured approximately 86.5 ± 0.7 % for the matrix systems and 90 ± 0.8 % for the core-shell systems. Moreover, the particle sizes of matrix systems were measured in the range of 2000–2100 mμ and the particle sizes of single-layer and double-layer reservoir systems were in the ranges of 1600–1700 mμ and 1500–1700 mμ, respectively. The study investigated the stability of curcumin in these systems under various environmental conditions, including exposure to light, heat, pH variations, ions, and storage. Results demonstrated that the presence of multiple layers significantly enhanced the drug's stability. Afterwards, swelling and drug release profiles were assessed in simulated gastric, intestinal, and colon fluids. The swelling of the matrix, single-layer and double-layer reservoir systems after 29 h were 127.4 %, 146.9 % and 144 %, respectively. The matrix system showed 68.7 % drug release after 29 h, whereas single-layer chitosan-shelled and double-layer chitosan/alginate-shelled reservoir systems released 51.8 % and 45.6 % of the drug, respectively. The release mechanism was explored using zero-order, Korsmeyer-Peppas, and Kopcha kinetic models. Comparative analysis of the experimental results and model fittings indicated a deviation from Fickian diffusion, with erosion becoming more pronounced with each additional layer. In conclusion, the system with a zein core and double-layer chitosan/alginate shell displayed effective drug release regulation and enhanced stability of curcumin, making it a promising candidate for efficient drug delivery.

1. Introduction

Curcumin, a yellowish polyphenolic compound, has captured considerable attention across diverse sectors, ranging from pharmaceuticals and food to cosmetics. This bioactive constituent occurs naturally within turmeric rhizome, which finds widespread usage in South Asian cuisine [1]. Through years of extensive research conducted by various scholars, it has become evident that curcumin

* Corresponding author.Polymer Engineering Department, Chemical Engineering Faculty, Tarbiat Modares University, P. O. Box No. 14115-114, Tehran, Iran.

E-mail addresses: Amitis.aghelinejad@modares.ac.ir (A. Aghelinejad), ebrahimn@modares.ac.ir (N. Golshan Ebrahimi).

exhibits antioxidant, anti-inflammatory, anticancer, antibacterial, antifungal, antiviral [1,2], anti-allergy [1], antimicrobial [3,4], anticoagulant [4,5], antiparasitic [5], antimalarial [2], and wound healing [2,4] properties. Furthermore, it displays potential as a safeguarding agent against cancer [3,4], Alzheimer's disease [3,5], diabetes [1,4], HIV infection [3], hypolipidemic effects [6], obesity [4], cardiovascular issues [3,4], and colorectal diseases [7]. Moreover, its remarkable safety profile is underscored by the absence of reported toxicity even at high dosages. This exceptional attribute has led to substantial interest in its potential therapeutic applications [3]. By way of example, numerous recent studies have been conducted to investigate curcumin's efficacy in treating COVID-19 patients. Notably, a team of researcher showcased curcumin's robust immune-modulating properties, suggesting its potential to ameliorate the inflammatory response associated with COVID-19 [8]. Additionally, another group claimed that curcumin could serve as a valuable supplementary option during the vaccination phase. This assertion stems from curcumin's capacity to enhance antibody production following vaccination [9]. Nevertheless, despite these notable attributes, the utilization of this bioactive compound encounters obstacles arising from its low water solubility (ranging from 3.14 μg mL^{-1} to 18.12 μg mL^{-1} [10]) and sensitivity to light, heat, alkaline media, and oxidation. Consequently, its oral bioavailability remains restricted at just 1 %, necessitating high dosages [4].

To overcome these limitations, various techniques have been employed, encompassing the design and encapsulation of curcumin within distinct delivery systems [11]. Proteins function as nutritional, cost-effective and safe carriers for curcumin, exhibiting the capability to enhance the stability and solubility of this bioactive compound [7]. Furthermore, it is noteworthy that proteins demonstrate greater effectiveness in controlling the release of encapsulated polyphenols compared to polysaccharides [12]. Nevertheless, the utilization of proteins in oral drug delivery systems is hindered by challenges such as enzymatic degradation and the acidic environment of the stomach [13]. To tackle these concerns and enhance protein stability within the aforementioned environments, a viable approach involves encapsulating the protein core with a polysaccharide coating [14]. Zein is a natural protein derived from corn, stands out as an edible, odorless, tasteless, biocompatible, and water-insoluble option [13]. Structurally, zein comprises a substantial portion of hydrophobic amino acids, with a comparatively smaller proportion consisting of hydrophilic amino acids [15]. Consequently, its incorporation as a carrier has the potential to enhance the bioavailability of poorly water-soluble drugs [16], and it exhibits efficacy in encapsulating hydrophobic anticancer agents for efficient release [13].

As previously indicated, the application of a polysaccharide coating to Zein has been highlighted for its potential to bolster protein stability within the gastrointestinal environment. Chitosan, a biocompatible and biodegradable compound, is derived from the deacetylation of chitin and presents two distinct structural units (amino and hydroxyl groups) amenable to modification [13]. This polysaccharide is antifungal, antibacterial, tissue regenerative, and coacervates with anion polysaccharides owing to its positive charge. In simpler terms, the opposing charges facilitate the formation of a polyelectrolyte complex between the two polysaccharides, leading to reduced porosity within the polymer network. As a result, chitosan can be coated with an anionic polysaccharide like alginate to create a complex endowed with this characteristic, thereby retarding the release of the drug encapsulated within the complex [17]. Due to its biodegradability, biocompatibility, and gelation characteristics, alginate finds application in drug delivery systems. Derived from brown algae, this bio-based polysaccharide is composed of mannuronic acid and guluronic acid monomers [13]. To encapsulate a drug within alginate, the cross-linking process involves the use of Ca^{2+} ions, which interact with the carboxylate groups of alginate, resulting in the formation of a calcium alginate gel [18]. The resultant calcium alginate gel forms a robust, heat-stable matrix that is cost-effective, non-toxic, and biocompatible with cells [19]. In acidic conditions, this substance transforms into a water-insoluble, condensed alginic acid hydrogel capable of regulating the release of an anticancer drug [13]. Furthermore, due to hydration within the mucus gel layer of the epithelial surface, the resulting particles adhere to mucosal surfaces, enhancing treatment efficacy [20]. However, this polysaccharide exhibits certain limitations as a drug delivery carrier, including issues such as swelling, erosion, low encapsulation efficiency, and rapid drug release [13]. To address these drawbacks, alginate can be employed in combination with other polysaccharides, such as chitosan [19].

In the current research, the focus is on fabricating drug delivery systems comprising a zein and curcumin core enveloped by a double-layer shell of chitosan and alginate. The core-shell system with a singular shell was crafted using an extrusion technique, involving vibrating, airflow, and concentric nozzles. Subsequently, the second layer was established through a coating process. Following the assembly of these systems, the influence of each layer on the release of curcumin and its stability across diverse conditions has been investigated.

2. Material and methods

2.1. Materials

The Zein, low molecular weight Chitosan, Sodium tripolyphosphate (STPP), Sodium Chloride (NaCl), Potassium dihydrogen phosphate (KH$_2$PO$_4$), Pepsin, and Pancreatin were purchased from Sigma-Aldrich. Curcumin (95 % purity) and Alginate were sourced from Shanghai Yuanye Bio-Technology Co., Ltd. Calcium chloride dihydrate, Acetic acid, Sodium Hydroxide (NaOH) (99.5 % purity), and Hydrochloric Acid (HCl) were obtained from Dr. Mojallali Industrial Chemical Complex Co. Furthermore, Ethanol (99.7 % purity) was supplied by Hamoon Teb Markazi Medicinal Chemical Industrial Co. Distilled water was employed in all experimental procedures.

2.2. Preparation of microparticles

To produce the microparticles, a coaxial airflow extrusion device provided by Dorsa-Iran was employed, equipped with a vibrating nozzle. The first group of microparticles, which contained curcumin-loaded zein matrix (CurZ), was generated using a 23-gauge needle (OD of 0.5 mm). The two other drug delivery systems, encompassing curcumin loaded within a core-shell configuration with a single

shell of Chitosan (CurZCS), and a core-shell structure with a double-layer shell of Chitosan and Alginate (CurZCSAlg), were created using two coaxial needles. The inner needle had a 23-gauge diameter, while the outer needle had a 16-gauge diameter (OD of 1.6 mm).

To generate the matrix system (CurZ), a solution of zein and curcumin (26 % and 1 % w/v) in 80 % ethanol-water was prepared and stirred at 800 rpm for 3.5 h. The concentration values of the polymer and drug, as well as the dissolution conditions, were predicated on prior investigations [21], aiming to ensure the thorough dissolution of both the polymer and drug, thus enabling the creation of effective pharmaceutical systems. The prepared polymeric solution was then injected into the device using a syringe pump (LSP01 model, Longer Company, China) at a velocity of 0.05 mm/s. The injected fluid entered the needle and dripped into a STPP solution with simultaneous airflow. The distance between the dripping system and the solidification bath was 4 cm.

To create the core-shell system with a single-layer shell (CurZCS), a solution of zein and curcumin (10 % and 1 % w/v) in 80 % ethanol-water was prepared and stirred at 800 rpm for 3.5 h. The prepared polymeric solution was injected into the inner needle using the above-mentioned syringe pump with a velocity of 0.07 mm/s. Simultaneously, a Chitosan solution (5 % w/v) in a 2 % acetic acid solution [22] was injected into the outer needle using a syringe pump (SATALAB company, Iran) with a velocity of 1.2 mm/s. After all, the injected fluid dripped into a STPP solution with simultaneous airflow. The spatial gap between the droplet release mechanism and the gelation bath was 4 cm.

To produce the core-shell system with a double-layer shell (CurZCSAlg), the pre-existing core-shell microparticles were initially subjected to a thorough rinse with distilled water. They were then mixed with an alginate solution (0.5 % w/v) at 200 rpm for 30 min. Subsequently, the microparticles underwent another round of washing with distilled water before being mixed with a solution of Calcium Chloride (2 % w/v) at 200 rpm for 10 min. The concentration values of alginate and calcium chloride concentration, as well as the time and stirring speed, were chosen based on previous studies [23–25] to ensure proper layering, crosslinking, and attainment of the desired spherical morphology of the particles.

As the injection rate and the distance between the dripping system and gelation bath have influences on microparticles [26–28], these factors were carefully determined through several production runs for the three types of above-mentioned microparticles (CurZ, CurZCS, and CurZCSAlg), considering the shape of the microparticles and the encapsulation efficiency of the drug.

2.3. Characteristics of drug-loaded microparticles

2.3.1. Infrared spectroscopy

The Infrared (IR) spectra of curcumin, zein, chitosan, alginate, CurZ, CurZCS, and CurZCSAlg particles after freeze-drying were obtained using a Frontier FTIR spectrometer (PerkinElmer Co., USA) [29]. The samples were prepared by mixing and pressing with potassium bromide onto a transparent pallet.

2.3.2. Size distribution and morphology observation

Initially, the dimensions and configurations of CurZ, CurZCS, and CurZCSAlg particles were examined using an optical microscope (Optikala, Nikkon Co., Japan). 30 particles from each category were randomly selected and analyzed thorough Dino Capture software to determine their dimensions and dispersion. Subsequently, the structure of CurZ, CurZCS, and CurZCSAlg particles was explored in greater detail using an AIS2100 scanning electron microscope (SEM) from SERON TECHNOLOGY, South Korea.

2.3.3. Encapsulation efficiency and loading efficiency of curcumin

The Encapsulation Efficiency (EE) and Loading Efficiency (LE) of curcumin within each particle type (CurZ, CurZCS, and CurZCSAlg) was determined using **Eq.** (1) [30] and **Eq.** (2) [31,32], respectively:

$$EE\% = \frac{\text{Loaded Curcmin in particles}}{\text{Curcumin added to Zein solution}} \times 100 \tag{1}$$

$$LE\% = \frac{\text{Loaded Curcmin in particles}}{\text{Weight of the particles}} \times 100 \tag{2}$$

To quantify the loaded curcumin and the initial curcumin added to the zein solution, the particles collected within a 30-s timeframe were subjected to three rounds of washing with distilled water. Subsequently, they were placed into a specific volume of 50 % ethanol solution. After 4 h, the particles were crushed [33–35], and they remained in the solution for an additional 4 h to ensure the complete dissolution of the drug. The curcumin content was then measured using a UV–Vis spectrometer at an absorbance of 430 nm, following the curcumin standard curve (Fig. S1). Additionally, the total amount of curcumin injected into the system was calculated based on the injection speed, duration, and concentration of the curcumin in the zein solution.

2.3.4. Stability

To assess the stability of each system under various conditions, a specific amount of each microparticle system was exposed to the following conditions that are discussed below. Then, the amount of drug in each system was determined using a UV–Vis spectrophotometer, and its ratio to the initial amount of loaded drug was calculated. To remove the time factor, all systems were subjected to a fixed time of 4 h in each environment, except during storage, where microparticles were kept for an extended period.

Stability against heat: The microparticles were placed in closed containers and exposed to a hot water bath with a temperature of 80 °C [11,21,36,37].

Stability against UV: The microparticles were placed in closed containers and exposed to a UV lamp (15W UVC) at a distance of 30

cm [21,38].

Stability against ion: The microparticles were immersed in a 2 M sodium chloride solution [39].

Stability against pH: The microparticles were placed in three solutions with different pH values (pH 3, distilled water, and pH 11) [10].

Stability during storage: The microparticles were stored in the refrigerator (4 °C) with and without the presence of distilled water for 24 days [40].

2.3.5. Swellability

To evaluate the swellability of each system under simulated gastrointestinal conditions (stomach (pH = 1.2), small intestine (pH = 6.8), and large intestine (pH = 7.4)), the initial mass of a specific quantity of particles in each system was measured. These separated particles were then placed in simulated gastric fluid (SGF) at 37 °C (consisting of 800 mL SGF with 1.6 g sodium chloride and 2.56 g pepsin [37]) for 2 h. After several washes with distilled water, the particles were transferred to simulated small intestine fluid (SIF) at 37 °C (containing 800 mL SIF with 5.44 g potassium dihydrogen phosphate, 7.04 g sodium chloride, 1.6 g pancreatin [37,41,42]) for 3 h. Subsequently, they underwent another round of washing and were subjected to simulated large intestine conditions at 37 °C for 24 h [41,42]. At specific time intervals, the mass of the particles in each type of system was measured and the swelling rate was calculated using Eq. (2) [17]:

$$(\%) \text{ swelling} = \frac{Mass \ of \ particles - Initial \ mass \ of \ particles}{Initial \ mass \ of \ particles} \times 100 \tag{3}$$

2.3.6. In vitro release kinetics analysis

The release of curcumin from each type of system under simulated gastrointestinal conditions (stomach (pH = 1.2), small intestine (pH = 6.8), and large intestine (pH = 7.4)) was determined using a UV–Vis spectrophotometer and the corresponding standard curves (Fig. S2). The release of curcumin from each system was investigated by gathering release content in simulated gastric fluid for 2 h, simulated small intestinal fluid for 3 h, and simulated large intestinal fluid for 24 h. During the initial 2 h in simulated gastric fluid, the drug release amount was monitored at 30-min intervals. After rinsing the particles with distilled water, they were transferred to simulated small intestinal fluid, and the release content was measured every 1 h. Following another round of washing with distilled water, the particles were moved to simulated large intestinal fluid, and the amount of released drug was measured at specific time points. To maintain a consistent volume, fresh release medium was added after each sampling of the drug release medium [41,42]. Subsequently, after obtaining the release rate graphs over time for each type of system, the drug release mechanism was explored using the mathematical models to describe the release kinetics of curcumin from CurZ, CurZCS, and CurZCSAlg microparticles under different digestion conditions [43,44]. Table 1 outlines the mathematical models employed to characterize the drug release kinetics.

3. Results and discussion

3.1. Structural analysis

3.1.1. FTIR

The Fourier transform infrared spectroscopy (FTIR) analysis was conducted to investigate the interactions in each of the constructed systems. The results of the FTIR are shown in Fig. 1(a) for curcumin (Cur), zein (Z), chitosan (CS), and alginate (Alg). Fig. 1 (b) displays the FTIR results for the fabricated systems, namely CurZ, CurZCS, and CurZCSAlg.

Comparing the results of the matrix system (CurZ) in Part II of Fig. 1(b) with the outcomes of separate zein and curcumin in Part I of Fig. 1(a) reveals the establishment of hydrogen bonds between the amide group of zein and the hydroxyl groups of curcumin [11,37]). It is worth mentioning that the broad peak within the 2900-2100 cm^{-1} range is attributed to the inclusion of TPP during the construction of this system [46]. Moreover, several peaks observed in the curcumin spectra (Part III) are absent in the matrix system (Part IV), likely due to the encapsulation of curcumin within the system and the confinement of its bonds under tension and bending effects [11]. The peaks corresponding to the amide I and amide II groups in zein, which are observed at wavenumbers of 1666 cm^{-1} and 1530

Table 1
Mathematical models to describe the release kinetics of the drug.

| Model	Equation	Constants	Description
Zero Order Model [45]	$Q = Q_0 + Kt$	Q = amount of drug released in time t Q_0 = initial amount of drug K = zero order release constant	–
Korsmeyer-Peppas Model [12, 45]	$Q = kt^n$	Q = amount of drug released in time t K = release rate constant n = diffusion expression	For spherical particles: n < 0.43 Fickian Diffusion 0.43<n < 0.85 Non-Fickian Diffusion 0.85<n < 1 Case II Transport
Kopcha Model [10]	$Q = A \times t^{0.5} + B \times t$	Q = amount of drug released in time t A = diffusional term coefficient B = erosional term coefficient	A/B >1 Diffusion A/B <1 Erosion
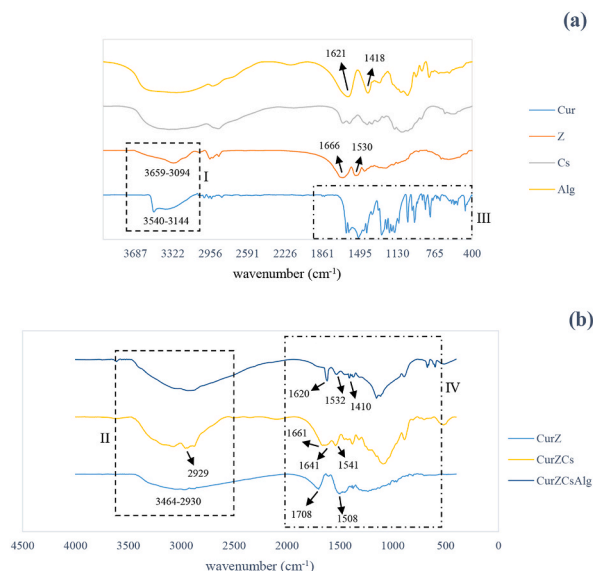
Fig. 1. FTIR (a) material, (b) CurZ, CurZCS, and CurZCSAlg systems (after freeze-drying of particles).

cm^{-1}, respectively [37], exhibit shifts to 1708 cm^{-1} and 1508 cm^{-1} in the matrix system. This shift can be attributed to hydrophobic interactions occurring between the nonpolar amino acid groups of zein and the hydrophobic curcumin [11,37]). Consequently, the matrix system composed of zein and curcumin demonstrates the presence of both hydrophobic and hydrogen interactions.

In the single-layer shell system (CurZCS), the FTIR results reveal the presence of an OH peak (in Part II), indicative of hydrogen bonds formed between the amide groups of zein and the hydroxyl groups of curcumin [11,37]. Additionally, the peak observed at the wavenumber of 2929 cm^{-1} can be attributed to the C–H tension in the components of the system [29]. Also, the shift of the amide II groups peak from the wavenumber of 1530 cm^{-1} to 1541 cm^{-1} indicates occurrence of electrostatic interactions between zein and chitosan [11]. The peak corresponding to amide I groups is divided into two distinct peaks at the wavenumbers of 1641 cm^{-1} and 1661 cm^{-1}, which can be attributed to ionic interactions between TPP and chitosan [47]. In addition, the absence of most of the curcumin-related peaks indicates successful encapsulation of curcumin within the system [11]. Thus, the formation of this system involves a combination of hydrophobic, hydrogen, and electrostatic interactions.

In the core-shell system with a double-layer shell (CurZCSAlg), the FTIR results reveal peak shifts for the symmetric and asymmetric carboxyl groups of alginate, as well as the amide II groups of chitosan, occurring at wavenumbers of 1620 cm^{-1}, 1410 cm^{-1} and 1532 cm^{-1}, respectively. These shifts suggest the presence of electrostatic interactions between alginate and chitosan [42,48]. Hence, in addition to the previously mentioned interactions, the construction of this system also involves the incorporation of electrostatic interactions between alginate and chitosan.

3.1.2. Particle size and morphology

The particle size distribution for each type of system is depicted in Fig. 2. The utilization of coaxial airflow in the production process facilitated the formation of droplets. Moreover, the implementation of vibration technology led to fragmentation of the laminar fluid
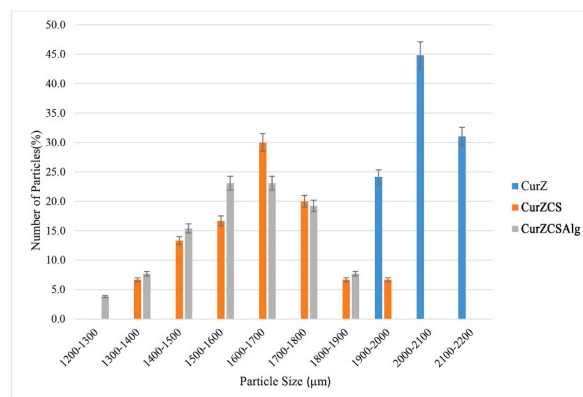

Fig. 2. Dispersity of the size of particles by measuring 30 randomly selected particles from each type of systems (CurZ, CurZCS, CurZCSAlg).

jet into uniformly sized droplets [25]. Skop et al. demonstrated that coaxial airflow can significantly reduce the size of chitosan microspheres [49]. Furthermore, Prusse et al. demonstrated that both coaxial airflow and vibration technology have the potential to decrease the size of alginate microparticles. They also highlighted the influence of the alginate solution concentration on the size and process efficiency during the extrusion method [50]. According to Fig. 2, the particle sizes within the matrix system (CurZ) were primarily distributed in the range of 2000–2100 mμ. In contrast, the particle sizes of CurZCS and CurZCSAlg systems predominantly fell within the ranges of 1600–1700 mμ and 1500–1700 mμ, respectively.

The notable larger size of particles within the matrix system compared to the two other systems can be attributed to the substantially higher concentration of the injected solution in this particular system [27]. As a consequence, the efficiency of the airflow and vibration during the extrusion process diminishes, leading to the formation of larger particles [25]. Within the CurZCSAlg system, the microcapsules exhibited a size range spanning from 1200 to 1900 mμ, while the particle size range observed in the CurZCS systems fell within 1300–2000 mμ. Employing Microsoft Excel and considering the possibility that these two data sets are identical, the calculated P-value was found to be 0.15. Conversely, if it is assumed that these data sets differ, the resultant P-value remains at 0.15. Consequently, neither hypothesis can be accepted, as the P-value fails to fall below the threshold of 0.05. As a conclusion, it can be deduced that these two sets of data exhibit minimal differences from one another [51,52]. However, upon the introduction of the alginate layer, the average particle size exhibited a reduction from 1638.93 mμ to 1579.848 mμ. This diminution in size could potentially be attributed to the observed electrostatic interaction between alginate and chitosan, as illustrated in Fig. 1. The establishment of electrostatic interaction likely leads to the attraction of the carboxyl group of alginate toward the amino group of chitosan [53–55]. Consequently, a reduction in particle size might occur as a result of this interaction. It is worth noting that since the media's pH is not alkaline and the chitosan layer's thickness significantly surpasses that of alginate, a conspicuous disparity in size between these two groups of particles is not apparent. The images of these constructed systems, both sectioned and unsectioned, under the
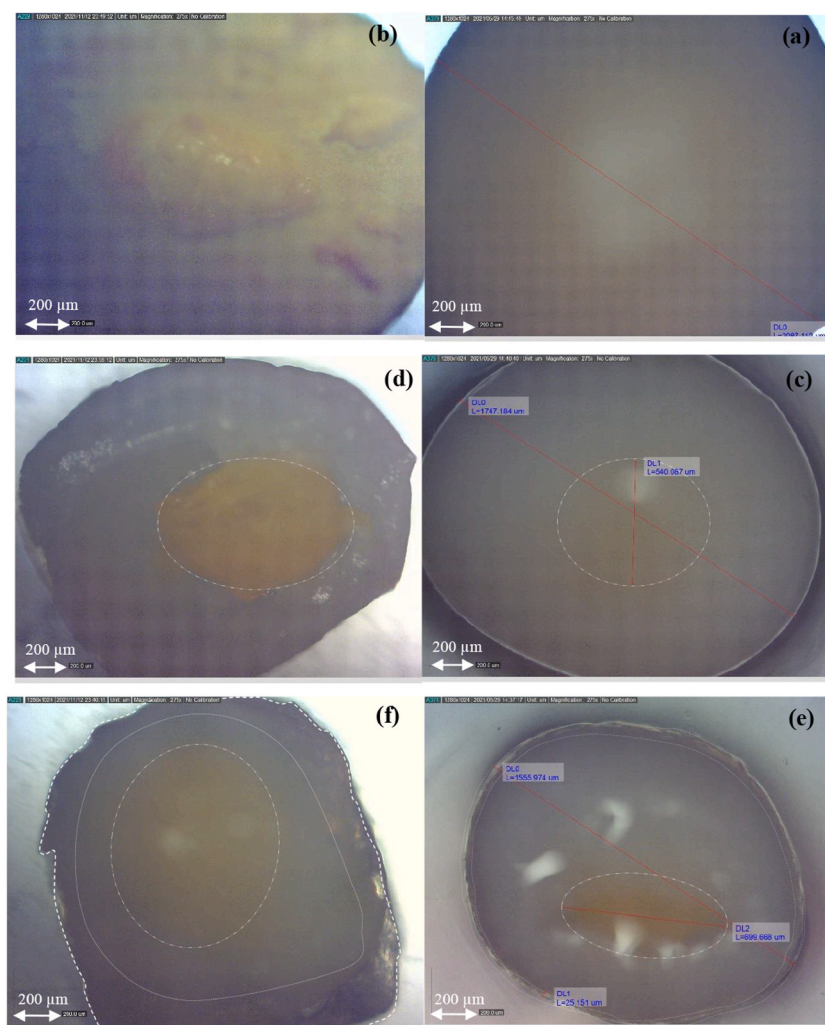

Fig. 3. Analyzing shape and size of freshly produced microcapsules under optical microscope (a) CurZ system, (b) halved CurZ system, (c) CurZCS system, (d) halved CurZCS system, (e) CurZCSAlg system, and (f) halved CurZCSAlg system.

microscope are depicted in Fig. 3.

The morphology of the freeze-dried particles analyzed by scanning electron microscopy is shown in Fig. 4. In the matrix system, as seen in Fig. 4(a) and (b), numerous pores are evident, indicating a porous structure. However, in particles with the chitosan layer (CusZCs), as shown in Fig. 4(c) and (d), the pore size is smaller compared to the previous type of particles. This reduction in pore size may be attributed to the crosslinking between TPP and Chitosan [56–58]. It's important to note that during the cutting and preparation of the particle for freeze-drying, tension was exerted on the particle, causing its layers to separate. In the image of the particle with the dual shell (CurZCSAlg), as shown in Fig. 4(e) and (f), the alginate layer is clearly visible. This outcome is a result of the electrostatic interaction between Chitosan and Alginate [40].

3.1.3. Encapsulation efficiency and loading efficiency

The encapsulation efficiency and loading efficiency of curcumin was approximately 86.5 ± 0.7 % and 3.2 % for the matrix systems (CurZ), respectively, and 90 ± 0.8 % and 1.1 %, respectively, for the core-shell systems (CurZCS and CurZCSAlg). The higher EE observed in the core-shell systems can be attributed to the structure of the system [12]. Moreover, within the core-shell system, the core of zein and the shell of chitosan function as barriers, preventing the drug from escaping the system during the preparation process. This additional obstacle presented by the shell, as compared to the matrix system, facilitates greater drug retention within the system, thereby leading to a heightened EE.
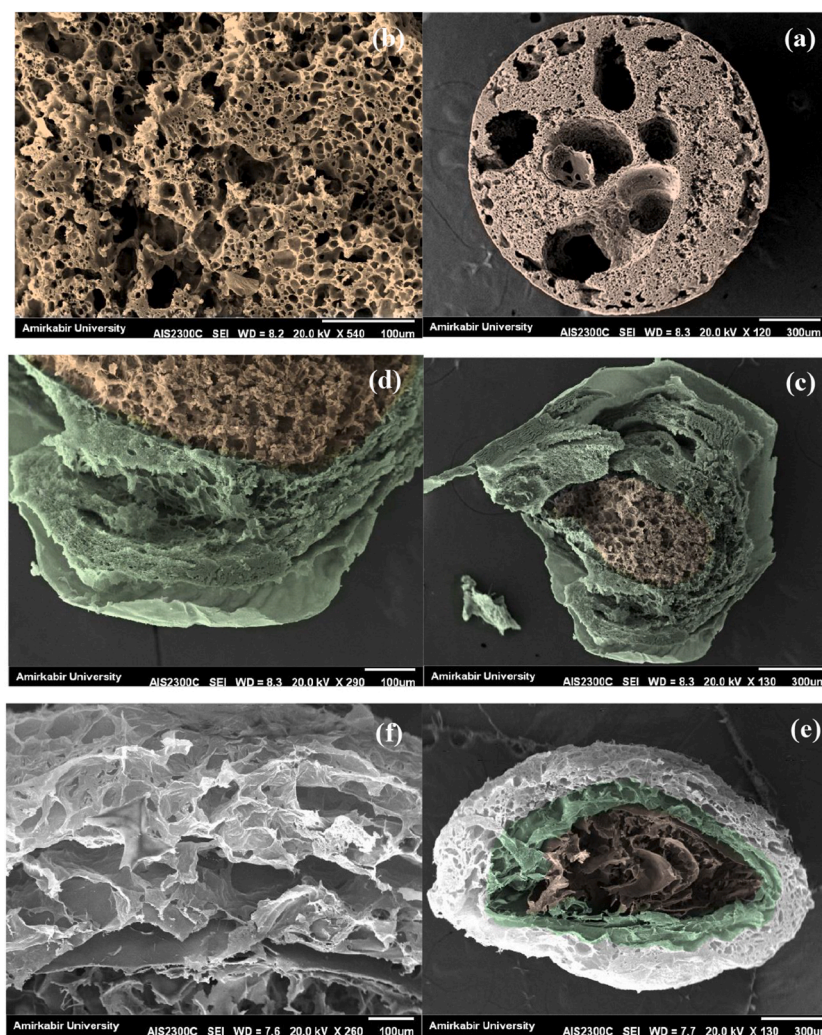

Fig. 4. SEM images of the freeze-dried particles, (a, b) CurZ system, (c, d) CurZCS system, (e, f) CurZCSAlg system (Parts (a), (c), and (e) with a magnification of 300 μm and parts (b), (d), and (f) with a magnification of 100 μm).

3.2. Stability

3.2.1. Effect of heating

Curcumin is recognized for its susceptibility to thermal degradation, and the rate of this degradation exhibits variability based on temperature. Based on the conducted studies that have examined curcumin's degradation up to 90 °C, the most notable degradation rates are observed within the temperature range of 70–90 °C. It's noteworthy that the reported degradation values within this range are approximately consistent [36,59]. Hence, other investigations have explored curcumin degradation at an 80 °C temperature [11,37]. Notably, Sun et al. reported that only about 15 % of curcumin remained after 4 h at 80 °C [60]. In contrast, the curcumin content retained within the developed microcapsules in this study was considerably higher, as depicted in Fig. 5. These findings suggest that the inclusion of chitosan and alginate contributes to enhancing curcumin's stability against heat due to the structural transformation from a matrix configuration to a core-shell system [61]. Furthermore, the establishment of a dense coating due to the aforementioned interactions, such as cross-linking, leads to the protection of curcumin against heat [37]. Importantly, with the inclusion of each layer, the transfer of heat to the particle's core requires more time [62], contributing to a larger portion of curcumin remaining within a specific duration (4 h).

3.2.2. Effect of UV

Curcumin possesses aromatic rings that render it prone to absorbing UV light, leading to accelerated degradation [21]. A study conducted by Sun et al. revealed that following an hour of UV exposure, only 20 % of curcumin remained intact [60]. However, the present study demonstrates a markedly higher amount of curcumin remaining after 4 h of UV exposure in each type of fabricated system, as illustrated in Fig. 6. The incorporation of each layer leads to an enhanced stability of curcumin against UV, which can be attributed not only to the structural modification of the system [61], but also to the presence of amino acid groups and dual linkages in Zein, alongside aromatic groups and dual linkages in chitosan and alginate. These mentioned groups effectively absorb UV radiation and mitigate curcumin degradation [29].

3.2.3. Stability against pH

Curcumin is susceptible to degradation in environments with both alkaline and low pH conditions, attributed to protonation processes [10]. In the current study, the stability of curcumin in acidic, alkaline, and deionized water was investigated. The results are shown in Fig. 7. The inclusion of the chitosan layer led to a reduction in the degradation of curcumin, particularly evident in alkaline media. This phenomenon can be attributed to the structural transformations from the matrix system to the core-shell configuration [61]. The enhanced stability can also be attributed to the insolubility of chitosan in alkaline media, along with the interactions discussed earlier [17,63]. The introduction of the alginate layer presents an additional decline in curcumin degradation, particularly noticeable in acidic media. This effect is attributed to the insolubility and shrinkage of the alginate layer under acidic pH conditions, as well as the electrostatic interactions between chitosan and alginate [13,17].

3.2.4. Stability against ion

The presence of OH^- ions contributes to the degradation of curcumin, and the introduction of NaCl into water generates Cl^- ions, intensifying the process of curcumin degradation. As the concentration of these ions elevates in the medium, the rate of curcumin degradation escalates as well. In line with the investigations by Mondal et al., the curcumin that remained in a 2 M NaCl solution after 4 h was approximately 22 % [59]. In contrast, our study, employing comparable media and time duration, reveals a significant retention of curcumin in each system, as depicted in Fig. 8. This enhanced stability can be attributed to structural modifications [61] and the positive charge of chitosan, which attracts negatively charged ions and thus hinders curcumin degradation. Furthermore, the alginate layer repels negatively charged ions owing to its own negative charge [17].

3.2.5. Storage stability

Curcumin is known to be unstable against temperature, oxygen, light, and during storage [64]. Hence, an assessment of curcumin's
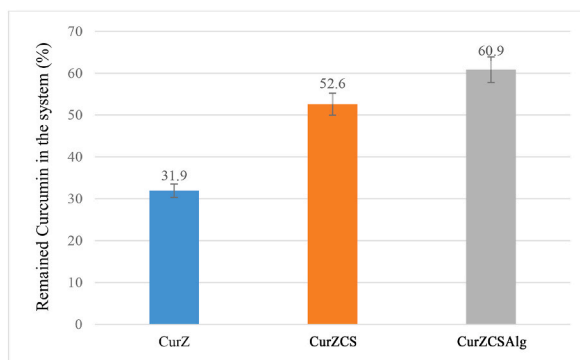
Fig. 5. The stability of Curcumin in each of the fabricated microparticles against heat (80 °C water bath for 4 h).
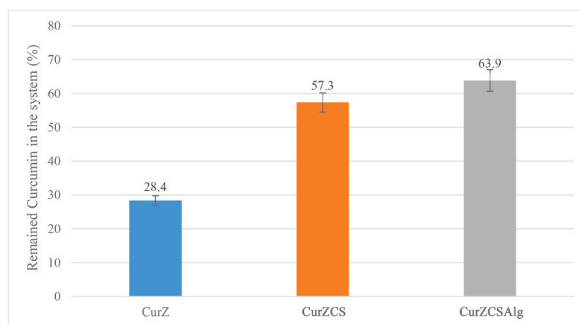
Fig. 6. The stability of Curcumin in each of the fabricated microparticles against UV light (15W UVC at a distance of 30 cm for 4 h).
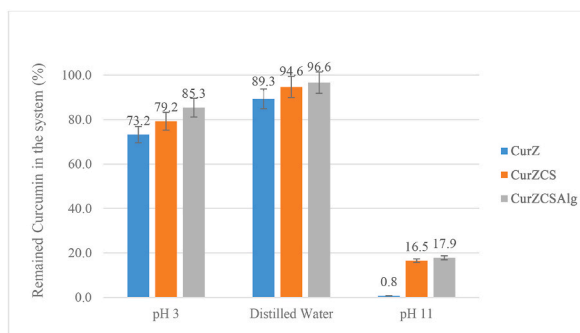

Fig. 7. The stability of Curcumin in each of the fabricated microparticles against pH (three solutions with different pH values (3, distilled water, 11) for 4 h).
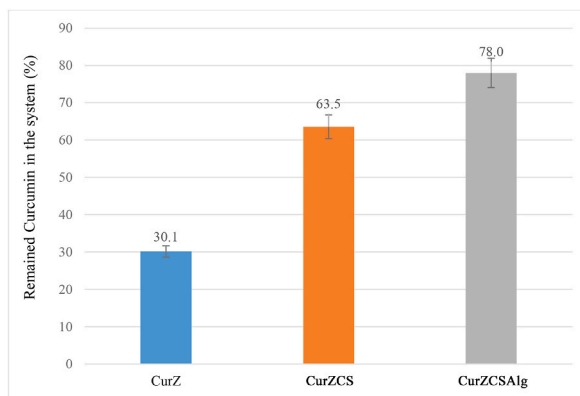

Fig. 8. The stability of Curcumin in each of the fabricated microparticles against ion (in a 2 M sodium chloride solution for 4 h).

stability within each of the fabricated systems was conducted over a span of 24 days. Furthermore, in order to mitigate curcumin degradation caused by heat and light, the produced particles were stored in a refrigerator at a temperature of 4 °C, shielded from light exposure [40]. Meng et al.'s research indicates that under similar conditions, 60 % of curcumin remains (in solution form) [4]. However, the present study investigated the stability of curcumin within each system in both deionized water and dried form. The inclusion of each layer led to an increase in the remaining curcumin due to the structural alterations [61]. Furthermore, the stability of curcumin in the dried form exceeded its stability in deionized water. This phenomenon could be attributed to the fact that molecules of water could penetrate the system when the particles were in the water, interacts with the drug, and result in more degradation in comparison with the dried form. Fig. 9 shows the remained curcumin in each system and media.

3.3. Swellability

The swellability of each type of system was investigated under simulated gastrointestinal conditions, and the results are illustrated
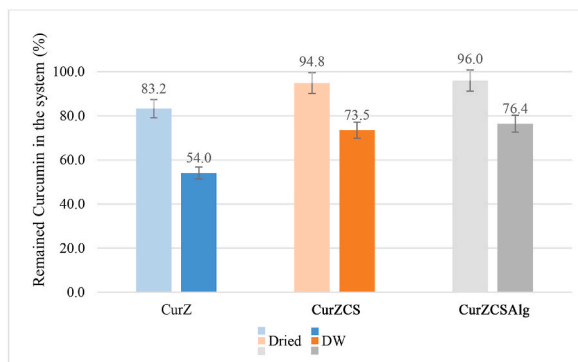
Fig. 9. The stability of Curcumin in each of the fabricated microparticles during storage in a refrigerator (4 °C) and in the absence of light for 24 days (in the distilled water and dried form).

in Fig. 10. The matrix system (CurZ) exhibited swelling of 118.9 %, 124.8 %, and 127.4 % in simulated stomach, small intestine, and large intestine media, respectively. Conversely, the core-shell system with the chitosan layer (CurZCS) underwent swelling of 143.5 %, 145.6 %, and 146.9 % in the corresponding media. Notably, the core-shell system displayed a greater increase in size compared to the expansion percentage of the matrix system in acidic media. This phenomenon might be attributed to the solubility of chitosan in the pH of the simulated stomach medium [17]. As the core-shell system with the chitosan layer was exposed to simulated intestinal media, the amino groups of chitosan underwent deprotonation, leading to a reduction in size [65]. When the alginate layer was introduced to the core-shell system (CurZCSAlg), the swelling of 135.9 %, 142.4 % and 144 % was measured. The diminished swelling compared to the core-shell system with a single layer of chitosan (CurZCS) can be attributed to the behavior of alginate in acidic media. Alginate acts as a weak polyacid, causing its polymer chains to come closer together due to protonated carbonyl groups and neutral chains [66]. Consequently, the potential for diffusion of the release media into the system was diminished, leading to reduced swellability.

3.4. Release

The release of curcumin from each type of system in simulated gastrointestinal media was thoroughly investigated by gathering release content. In Fig. 11(a), the curcumin release profile from the matrix system (CurZ) is depicted. Initially, a predetermined quantity of the prepared systems was introduced into the simulated stomach media (pH = 1.2). Following 2 h, approximately 50.2 % of the encapsulated curcumin was released. Subsequently, upon transferring these systems to the simulated small intestine media (pH = 6.8), the release content after 3 h was 13.7 % and the cumulative released drug content increased to 63.9 %. Continuing this sequence, after the transition to the simulated large intestine media (pH = 7.4), the release content was 4.8 % in 24 h and the cumulative released drug content further escalated to 68.7 %. Therefore, the release efficiency of the drug from this system was measured 68.7 % over 29 h. The release data were subjected to fitting using the models outlined in Table 1. Evaluating the coefficient of determination obtained (as detailed in Table 2), it becomes evident that the zero-order model does not aptly describe the release behavior, while the Kopcha model exhibits superior efficacy in depicting the drug release behavior from the matrix system, outperforming the Korsmeyer-Peppas model. Notably, the calculated A/B ratio within the Kopcha model surpassing 1 suggests that the system erosion has a relatively limited impact on drug release [10]. Furthermore, in the context of the Korsmeyer-Peppas model (n is equal to 0.58), the diffusion mechanism governing this release phenomenon is classified as non-Fickian [12,45].

Likewise, Fig. 11(b) illustrates the curcumin release profile from the core-shell system with the chitosan layer (CurZCS). Following a 2-h exposure to simulated stomach media (pH = 1.2), approximately 33 % of the encapsulated curcumin was released. Subsequently,
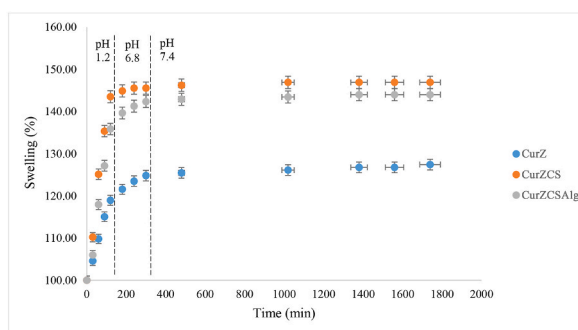

Fig. 10. The swelling behavior of each type of the microparticles in the simulated stomach (pH 1.2), small intestine (pH 6.8) and large intestine media (pH 7.4) for 2, 3 and 24 h, respectively, at 37 °C.
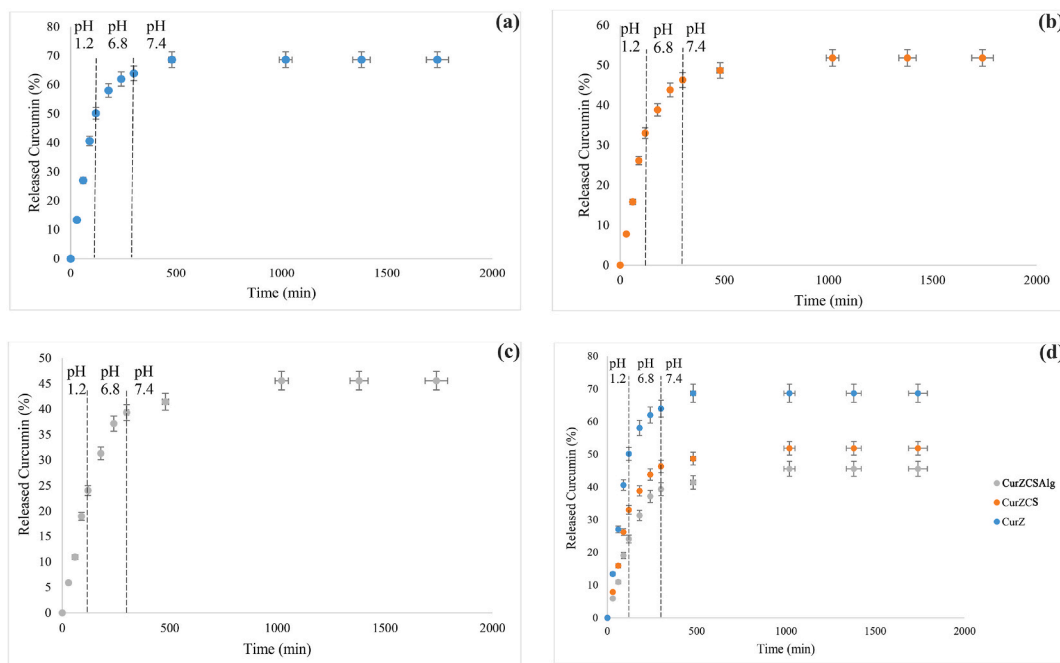
Fig. 11. The Curcumin release curve in simulated stomach (pH 1.2), small intestine (pH 6.8) and large intestine media (pH 7.4) for 2, 3 and 24 h, respectively, at 37 °C from (a) the CurZ system (b) the CurZCS system, (c) the CurZCSAlg system, and (d) comparison of the Curcumin release curves from each system in terms of time.

Table 2
The obtained coefficients of determination and constants from fitting the release data from each system to the mentioned models.

Microparticle	Model	Constants	R^2
CurZ	Zero-Order	K = 0.05	0.45
	Korsmeyer-Peppas	K = 2.47, n = 0.58	0.88
	Kopcha	A = 4.88, B = 0.07	0.95
CurZCS	Zero-Order	K = 0.04	0.53
	Korsmeyer-Peppas	K = 1.09, n = 0.67	0.9
	Kopcha	A = 3.42, B = 0.05	0.94
CurZCSAlg	Zero-Order	K = 0.04	0.59
	Korsmeyer-Peppas	K = 0.57, n = 0.74	0.93
	Kopcha	A = 2.63, B = 0.04	0.93

within 3 h of immersion in simulated small intestine media (pH = 6.8), a release content of 13.3 % and a cumulative release of 46.3 % of the curcumin were observed. The cumulative release escalated to 51.8 % after 24 h in the simulated large intestine media (pH = 7.4) and the release content during this period was 5.5 %. Therefore, the release efficiency of the drug from CurZCS system was 51.8 % during 29 h. The release mechanism within this system was investigated through the analysis of curcumin release data using the aforementioned models. Based on the coefficient of determination values acquired (as outlined in Table 2), it can be inferred that the zero-order model inadequately characterizes the release behavior. The Kopcha model demonstrates a higher efficacy in describing the curcumin release from the CurZCS system when compared to the Korsmeyer-Peppas model. In line with both the Kopcha and Korsmeyer-Peppas models, the release of curcumin from this system is predominantly governed by factors other than system erosion [10], and the diffusion process follows a non-Fickian pattern [12,45].

In Fig. 11(c), the release profile of curcumin from the core-shell system featuring both the chitosan and alginate layers (CurZCSAlg) is depicted. During 2, 3 and 24 h of immersing in each respective release medium the release content was measured at 24 %, 15.3 % and 6.3 % and the cumulative amount of drug released was 24 %, 39.3 %, and 45.6 %, respectively. Therefore the release efficiency of the drug from CurZCSAlg system was 45.6 % after 29 h. An examination of the release mechanism within this system is undertaken by assessing the fitting of the release data to the models enumerated in Table 1. After analyzing the calculated coefficients of determination (as presented in Table 2), it is evident that the zero-order model inadequately characterizes the release behavior. In contrast, the Korsmeyer-Peppas and Kopcha models effectively capture the drug release dynamics within our system. Additionally, when considering the Kopcha model and observing an A/B ratio exceeding 1, it can be inferred that system erosion does not exert a substantial influence on the release process [10]. Moreover, by taking into account the n value derived from the Korsmeyer-Peppas model, the observed release mechanism aligns with a non-Fickian diffusion behavior [12,45].

Fig. 11(d) offers a comparative visualization of the drug release profiles across each system type with respect to time. Notably, an evident trend emerges: with an increasing number of layers in the system, the drug release rate diminishes, and the initiation of release exhibits a more gradual slope. Moreover, upon analyzing the results from fitting the release data to the Korsmeyer-Peppas model, it becomes apparent that the values of n exhibit an upward trend upon the incorporation of each additional layer. This observation implies a departure from Fickian diffusion with the successive addition of each layer, leading to a more regulated and controlled drug release mechanism. This inference is further substantiated when assessing the determination coefficient values derived from the zero-order model fits, considering the suitability of this model in describing controlled release scenarios. Upon analyzing the data fitted with the Kopcha model, it becomes evident that erosion mechanisms do not significantly influence all three systems. However, it is noteworthy that the A/B ratio decreases with the incorporation of each successive layer. Consequently, in the case of the CurZCSAlg system, the contribution of the erosion mechanism to curcumin release holds greater significance compared to the other two systems.

The CurZCS system exhibits a greater degree of swelling in the release environment compared to the CurZ system. Chitosan, known to swell in the stomach environment [67], experiences enhanced interaction with the release environment. This augmented interaction hinders the diffusion of molecules from the release medium into the core, subsequently affecting core swelling and interaction with the drug for release. Consequently, the erosion mechanism gains slightly more prominence relative to the diffusion mechanism, leading to a release pattern characterized by a gentler slope [68,69]. Indeed, the decrease in drug release observed in the CurZCS system compared to the CurZ system can be attributed to the incorporation of the chitosan layer and the subsequent interactions that were evident in the FTIR analysis. Furthermore, the transformation of the matrix structure into a reservoir system has led to a more regulated and controlled release of the drug from the system [61]. In this system, the release of curcumin in the simulated small intestinal (pH = 6.8) and large intestinal (pH = 7.4) media exhibits a notably slower pace. This phenomenon can be attributed to the heightened stability and decreased solubility of chitosan in these particular environments [17]. In these media, the chitosan chains tend to congregate, creating a more compact structure. Consequently, the diffusion and release of the drug molecules through the densely packed chitosan chains are hindered, resulting in the observed slower release profile.

In the CurZCSAlg system, along with the interactions established among the system components and the presence of a reservoir structure with two shells [61], the utilization of alginate in the final layer exerted control over the release rate. Within this system, the release in the pH = 1.2 environment was lower compared to the other two systems. Alginate, being a weak polyacid, undergoes protonation of its carboxyl group and experiences a reduction in the ionic properties of its polymer chains within an acidic environment. As a consequence, the polymer chains congregate more closely, resulting in a decrease in release [66]. Hence, it functions as a barrier layer, diminishing the expansion of chitosan within an acidic environment. Consequently, in comparison to the preceding system, fewer molecules from the release medium are able to infiltrate the system, reach the core, and prompt its expansion for drug release through diffusion. Consequently, a greater portion of the molecules from the release environment is engaged in the erosion of the system, leading to an amplified contribution of the erosion mechanism. As a result, the release occurs with a shallower slope compared to the other two systems [68,69]. Finally, within the simulated small intestinal (pH = 6.8) and large intestine (pH = 7.4) media, the presence of sodium ions in the release medium and their replacement with calcium ions contribute to the disintegration of the polymer network [66]. Nevertheless, the presence of the chitosan layer, known for its stability under alkaline conditions [61], results in a gradual release process within these particular media.

Among the investigated systems, the CurZCSAlg microparticles demonstrate suitability for oral drug delivery purposes owing to their controlled drug release profile in the gastrointestinal environment, as well as the enhanced stability of curcumin against factors like heat, ions, pH variations, light exposure, and storage conditions. The presence of multiple layers in the core-shell system contributes to a controlled drug release mechanism, thereby establishing these systems as promising contenders for various drug delivery applications.

4. Conclusion

In conclusion, this study successfully developed three distinct drug delivery systems through the utilization of the extrusion method coupled with vibration and airflow techniques. The creation of core-shell systems necessitated the alteration of the extrusion nozzle to adopt concentric nozzles. Furthermore, the formation of the double-layer shell in the core-shell system was achieved employing a coating approach. Following the assembly of these systems, the impact of each layer's presence on microparticle size, stability, and drug release rate was thoroughly examined. The findings indicated that the core-shell systems with the double-layer shell of chitosan and alginate exhibited superior performance in curtailing drug release and enhancing curcumin's stability across diverse environmental contexts, including storage. The incorporation of individual layers within the core-shell systems yielded a decrease in microparticle size and heightened curcumin's stability against heat, light, pH variations, and ions. Furthermore, the analysis of drug release and swelling patterns in simulated gastrointestinal environments indicated a noticeable trend: with an increase in the number of layers among these systems, the initiation of drug release exhibited a gentler slope, accompanied by reduced quantities of released drug. Furthermore, upon analyzing the fitted release data using the Zero-order, Kopcha, and Korsmeyer-Peppas models, a notable trend emerged. With the introduction of each layer, the release mechanism exhibited reduced Fickian behavior, indicating enhanced control over drug release and an increased role of system erosion. In summary, the core-shell systems featuring a zein core and a double-layer shell of chitosan and alginate showcase potential as promising drug delivery platforms for oral administration of Curcumin. These systems provide superior control over drug release kinetics and bolstered stability, thereby positioning them as viable candidates for various pharmaceutical applications.

Data availability statement

Data included in article/supp. material/referenced in article.

Formatting of funding sources

CRediT authorship contribution statement

Amitis Aghelinejad: Writing – review & editing, Writing – original draft, Methodology, Investigation, Conceptualization. **Nadereh Golshan Ebrahimi:** Writing – review & editing, Supervision, Project administration, Methodology, Investigation, Funding acquisition, Conceptualization.

Declaration of competing interest

The authors declare that they have no known competing financial interests or personal relationships that could have appeared to influence the work reported in this paper.

Acknowledgment

Appendix A. Supplementary data

Supplementary data to this article can be found online at https://doi.org/10.1016/j.heliyon.2024.e33205.

References

[1] J. Lucas, M. Ralaivao, B.N. Estevinho, F. Rocha, A new approach for the microencapsulation of curcumin by a spray drying method, in order to value food products, Powder Technol. 362 (2020) 428–435, https://doi.org/10.1016/j.powtec.2019.11.095.

[2] O.S. Reddy, M.C.S. Subha, T. Jithendra, C. Madhavi, K.C. Rao, Curcumin encapsulated dual cross linked sodium alginate/montmorillonite polymeric composite beads for controlled drug delivery, Journal of pharmaceutical analysis 11 (2) (2021) 191–199, https://doi.org/10.1016/j.jpha.2020.07.002.

[3] H.R. Kavousi, M. Fathi, S.A. Goli, Novel cress seed mucilage and sodium caseinate microparticles for encapsulation of curcumin: an approach for controlled release, Food Bioprod. Process. 110 (2018) 126–135, https://doi.org/10.1016/j.fbp.2018.05.004.

[4] F.B. Meng, Q. Zhang, Y.C. Li, J.J. Li, D.Y. Liu, L.X. Peng, Konjac glucomannan octenyl succinate as a novel encapsulation wall material to improve curcumin stability and bioavailability, Carbohydr. Polym. 238 (2020) 116193, https://doi.org/10.1016/j.carbpol.2020.116193.

[5] A. Rezaei, A. Nasirpour, Evaluation of release kinetics and mechanisms of curcumin and curcumin-β-cyclodextrin inclusion complex incorporated in electrospun almond gum/PVA nanofibers in simulated saliva and simulated gastrointestinal conditions, BioNanoScience 9 (2019) 438–445, https://doi.org/10.1007/s12668-019-00620-4.

[6] L. Wu, J. Tian, X. Ye, H. Fang, Z. Zhang, C. Xu, H. Zhang, Encapsulation and release of curcumin with the mixture of porous rice starch and xanthan gum, Starch Staerke 73 (1–2) (2021) 2000042, https://doi.org/10.1002/star.202000042.

[7] F. Alavi, Z. Emam-Djomeh, M.S. Yarmand, M. Salami, S. Momen, A.A. Moosavi-Movahedi, Cold gelation of curcumin loaded whey protein aggregates mixed with k-carrageenan: impact of gel microstructure on the gastrointestinal fate of curcumin, Food Hydrocolloids 85 (2018) 267–280, https://doi.org/10.1016/j.foodhyd.2018.07.012.

[8] B. Abdelazeem, A.K. Awad, M.A. Elbadawy, N. Manasrah, B. Malik, A. Yousaf, S. Alqasem, S. Banour, S.M. Abdelmohsen, The effects of curcumin as dietary supplement for patients with COVID-19: a systematic review of randomized clinical trials, Drug Discoveries & Therapeutics 16 (1) (2022) 14–22, https://doi.org/10.5582/ddt.2022.01017.

[9] S.S. Widjaja, R. Rusdiana, R. Amelia, Curcumin: Boosting the immunity of COVID-19-vaccinated populations, \"J. Adv. Pharm. Technol. Research\"\" (JAPTR)\" 13 (3) (2022) 187, https://doi.org/10.4103/japtr.japtr_54_22.

[10] A. Patel, Y. Hu, J.K. Tiwari, K.P. Velikov, Synthesis and characterisation of zein–curcumin colloidal particles, Soft Matter 6 (24) (2010) 6192–6199, https://doi.org/10.1039/C0SM00800A.

[11] S. Chen, Y. Han, L. Jian, W. Liao, Y. Zhang, Y. Gao, Fabrication, characterization, physicochemical stability of zein-chitosan nanocomplex for co-encapsulating curcumin and resveratrol, Carbohydr. Polym. 236 (2020) 116090, https://doi.org/10.1016/j.carbpol.2020.116090.

[12] F.P. Flores, F. Kong, In vitro release kinetics of microencapsulated materials and the effect of the food matrix, Annu. Rev. Food Sci. Technol. 8 (2017) 237–259, https://doi.org/10.1146/annurev-food-030216-025720.

[13] R. Ahmad, Y. Deng, R. Singh, M. Hussain, M.A.A. Shah, S. Elingarami, N. He, Y. Sun, Cutting edge protein and carbohydrate-based materials for anticancer drug delivery, J. Biomed. Nanotechnol. 14 (1) (2018) 20–43, https://doi.org/10.1166/jbn.2018.2476.

[14] C. Chang, T. Wang, Q. Hu, Y. Luo, Caseinate-zein-polysaccharide complex nanoparticles as potential oral delivery vehicles for curcumin: effect of polysaccharide type and chemical cross-linking, Food Hydrocolloids 72 (2017) 254–262, https://doi.org/10.1016/j.foodhyd.2017.05.039.

[15] R. Paliwal, S. Palakurthi, Zein in controlled drug delivery and tissue engineering, J. Contr. Release 189 (2014) 108–122, https://doi.org/10.1016/j.jconrel.2014.06.036.

[16] P.H. Tran, W. Duan, B.J. Lee, T.T. Tran, The use of zein in the controlled release of poorly water-soluble drugs, Int. J. Pharm. 566 (2019) 557–564, https://doi.org/10.1016/j.ijpharm.2019.06.018.

[17] M. Lengyel, N. Kállai-Szabó, V. Antal, A.J. Laki, I. Antal, Microparticles, microspheres, and microcapsules for advanced drug delivery, Sci. Pharm. 87 (3) (2019) 20, https://doi.org/10.3390/scipharm87030020.

[18] A.S. Vaziri, I. Alemzadeh, M. Vossoughi, Improving survivability of Lactobacillus plantarum in alginate-chitosan beads reinforced by Na-tripolyphosphate dual cross-linking, Lebensm. Wiss. Technol. 97 (2018) 440–447, https://doi.org/10.1016/j.lwt.2018.07.037.

[19] V. Đorđević, A. Paraskevopoulou, F. Mantzouridou, S. Lalou, M. Pantić, B. Bugarski, V. Nedović, Encapsulation technologies for food industry. Emerging and traditional technologies for safe, healthy and quality food (2016) 329–382, https://doi.org/10.1007/978-3-319-24040-4_18.

[20] G. Kaur, J. Grewal, K. Jyoti, U.K. Jain, R. Chandra, J. Madan, Oral controlled and sustained drug delivery systems: concepts, advances, preclinical, and clinical status, in: Drug Targeting and Stimuli Sensitive Drug Delivery Systems, 2018, pp. 567–626, https://doi.org/10.1016/B978-0-12-813689-8.00015-X.

[21] Q. Liu, Y. Jing, C. Han, H. Zhang, Y. Tian, Encapsulation of curcumin in zein/caseinate/sodium alginate nanoparticles with improved physicochemical and controlled release properties, Food Hydrocolloids 93 (2019) 432–442, https://doi.org/10.1016/j.foodhyd.2019.02.003.

[22] D. Mark, S. Haeberle, R. Zengerle, J. Ducree, G.T. Vladisavljević, Manufacture of chitosan microbeads using centrifugally driven flow of gel-forming solutions through a polymeric micronozzle, J. Colloid Interface Sci. 336 (2) (2009) 634–641, https://doi.org/10.1016/j.jcis.2009.04.029.

[23] S.F. Lin, Y.C. Chen, R.N. Chen, L.C. Chen, H.O. Ho, Y.H. Tsung, M.T. Sheu, D.Z. Liu, Improving the stability of astaxanthin by microencapsulation in calcium alginate beads, PLoS One 11 (4) (2016) e0153685, https://doi.org/10.1371/journal.pone.0153685.

[24] E. Henao, E. Delgado, H. Contreras, G. Quintana, Polyelectrolyte complexation versus ionotropic gelation for chitosan-based hydrogels with carboxymethylcellulose, carboxymethyl starch, and alginic acid, Int. J. Chem. Eng. (2018), https://doi.org/10.1155/2018/3137167, 2018.

[25] U. Prüsse, L. Bilancetti, M. Bučko, B. Bugarski, J. Bukowski, P. Gemeiner, D. Lewińska, V. Manojlovic, B. Massart, C. Nastruzzi, V. Nedovic, Comparison of different technologies for alginate beads production, Chem. Pap. 62 (2008) 364–374, https://doi.org/10.2478/s11696-008-0035-x.

[26] R. Barbaz-Isfahani, S. Saber-Samandari, M. Salehi, Novel electrosprayed enhanced microcapsules with different nanoparticles containing healing agents in a single multicore microcapsule, Int. J. Biol. Macromol. 200 (2022) 532–542, https://doi.org/10.1016/j.ijbiomac.2022.01.084.

[27] A. Teimouri, R. Barbaz Isfahani, S. Saber-Samandari, M. Salehi, Experimental and numerical investigation on the effect of core-shell microcapsule sizes on mechanical properties of microcapsule-based polymers, J. Compos. Mater. 56 (18) (2022) 2879–2894, https://doi.org/10.1177/00219983221107831.

[28] R. Barbaz-Isfahani, S. Saber-Samandari, M. Salehi, Multi-scale modeling and experimental study on electrosprayed multicore microcapsule-based self-healing polymers, Mech. Adv. Mater. Struct. (2022) 1–14, https://doi.org/10.1080/15376494.2022.2162638.

[29] M.A. Khan, C. Yue, Z. Fang, S. Hu, H. Cheng, A.M. Bakry, L. Liang, Alginate/chitosan-coated zein nanoparticles for the delivery of resveratrol, J. Food Eng. 258 (2019) 45–53, https://doi.org/10.1016/j.jfoodeng.2019.04.010.

[30] A. Poshadri, K. Aparna, Microencapsulation technology: a review, Journal of Research ANGRAU 38 (1) (2010) 86–102. http://oar.icrisat.org/id/eprint/6375.

[31] L. Li, Z. Li, Y. Guo, K. Zhang, W. Mi, J. Liu, Preparation of uniform-sized GeXIVA[1,2]-loaded PLGA microspheres as long-effective release system with high encapsulation efficiency, Drug Deliv. 29 (1) (2022) 2283–2295, https://doi.org/10.1080/10717544.2022.2089297.

[32] H. Jin, H. Chong, Y. Zhu, M. Zhang, X. Li, N. Bazybek, Y. Wei, F. Gong, Y. He, G. Ma, Preparation and evaluation of amphipathic lipopeptide-loaded PLGA microspheres as sustained-release system for AIDS prevention, Eng. Life Sci. 20 (11) (2020) 476–484, https://doi.org/10.1002/elsc.202000026.

[33] M.R. Hussain, R.R. Devi, T.K. Maji, Controlled release of urea from chitosan microspheres prepared by emulsification and cross-linking method, Iran. Polym. J. (Engl. Ed.) 21 (2012) 473–479, https://doi.org/10.1007/s13726-012-0051-0.

[34] K.S. Patel, M.B. Patel, Preparation and evaluation of chitosan microspheres containing nicorandil, International journal of pharmaceutical investigation 4 (1) (2014) 32, https://doi.org/10.4103/2230-973X.127738.

[35] H. Kumar, M. Panwar, A. Kumar, S. Kumar, R. Jana, R. Rani, J. Roy, S. Ashique, Development and characterization of aripipraziole loaded solid lipid microparticles, J. Pharm. Negat. Results (2023) 78–98, https://doi.org/10.47750/pnr.2023.14.S01.10.

[36] Y. Liu, D. Liu, L. Zhu, Q. Gan, X. Le, Temperature-dependent structure stability and in vitro release of chitosan-coated curcumin liposome, Food Res. Int. 74 (2015) 97–105, https://doi.org/10.1016/j.foodres.2015.04.024.

[37] S. Chen, Q. Li, D.J. McClements, Y. Han, L. Dai, L. Mao, Y. Gao, Co-delivery of curcumin and piperine in zein-carrageenan core-shell nanoparticles: formation, structure, stability and in vitro gastrointestinal digestion, Food Hydrocolloids 99 (2020) 105334, https://doi.org/10.1016/j.foodhyd.2019.105334.

[38] F.N. Sorasitthiyanukarn, C. Muangnoi, P.R.N. Bhuket, P. Rojsitthisak, P. Rojsitthisak, Chitosan/alginate nanoparticles as a promising approach for oral delivery of curcumin diglutaric acid for cancer treatment, Mater. Sci. Eng. C 93 (2018) 178–190, https://doi.org/10.1016/j.msec.2018.07.069.

[39] X. Huang, X. Huang, Y. Gong, H. Xiao, D.J. McClements, K. Hu, Enhancement of curcumin water dispersibility and antioxidant activity using core–shell protein–polysaccharide nanoparticles, Food Res. Int. 87 (2016) 1–9, https://doi.org/10.1016/j.foodres.2016.06.009.

[40] M. Hasan, K. Elkhoury, C.J. Kahn, E. Arab-Tehrany, M. Linder, Preparation, characterization, and release kinetics of chitosan-coated nanoliposomes encapsulating curcumin in simulated environments, Molecules 24 (10) (2019) 2023, https://doi.org/10.3390/molecules24102023.

[41] J. Zhang, H.H. Li, Y.F. Chen, L.H. Chen, H.G. Tang, F.B. Kong, Y.X. Yao, X.M. Liu, Q. Lan, X.F. Yu, Microcapsulation of immunoglobulin Y: optimization with response surface morphology and controlled release during simulated gastrointestinal digestion, J. Zhejiang Univ. - Sci. B 21 (8) (2020) 611, https://doi.org/10.1631/jzus.B2000172.

[42] S. Maity, P. Mukhopadhyay, P.P. Kundu, A.S. Chakraborti, Alginate coated chitosan core-shell nanoparticles for efficient oral delivery of naringenin in diabetic animals—an in vitro and in vivo approach, Carbohydr. Polym. 170 (2017) 124–132, https://doi.org/10.1016/j.carbpol.2017.04.066.

[43] M. Shahrousvand, M. Hajikhani, L. Nazari, A. Aghelinejad, M. Shahrousvand, M. Irani, A. Rostami, Preparation of colloidal nanoparticles PVA-PHEMA from hydrolysis of copolymers of PVAc-PHEMA as anticancer drug carriers, Nanotechnology 33 (27) (2022) 275603, https://doi.org/10.1088/1361-6528/ac6089.

[44] M. Shahrousvand, N.G. Ebrahimi, Designing nanofibrous poly (ε-caprolactone)/hydroxypropyl cellulose/zinc oxide/Melilotus Officinalis wound dressings using response surface methodology, Int. J. Pharm. 629 (2022) 122338, https://doi.org/10.1016/j.ijpharm.2022.122338.

[45] D. Bhowmik, H. Gopinath, B.P. Kumar, S. Duraivel, K.S. Kumar, Controlled release drug delivery systems, Pharma Innov. 1 (10) (2012).

[46] S.Y. Azhary, D. Purnama, F.F. Florena, M. Vanitha, C. Panatarani, I.M. Joni, Synthesis and characterization of chitosan: SiO2 nanocomposite by ultrasonic spray drying, in: IOP Conference Series: Materials Science and Engineering (Vol. 550, No. 1, 012037, 2019, July, https://doi.org/10.1088/1757-899X/550/1/012037.

[47] B. Čalija, J. Milić, J. Janićijević, A. Daković, D. Krajišnik, Ionically cross-linked chitosan–halloysite composite microparticles for sustained drug release, Clay Miner. 52 (4) (2017) 413–426, https://doi.org/10.1180/claymin.2017.052.04.01.

[48] L.B. Sukhodub, H.O. Yanovska, V.M. Kuznetsov, O.O. Martyniuk, L.F. Sukhodub, Injectable biopolymer-hydroxyapatite hydrogels: obtaining and their characterization. http://essuir.sumdu.edu.ua/handle/123456789/44865, 2016.

[49] K. Lai, Y. How, L. Pui, Microencapsulation of Lactobacillus rhamnosus GG with flaxseed mucilage using co-extrusion technique, J. Microencapsul. 38 (2) (2021) 34–148, https://doi.org/10.1080/02652048.2020.1863490.

[50] N.B. Skop, F. Calderon, S.W. Levison, C.D. Gandhi, C.H. Cho, Heparin crosslinked chitosan microspheres for the delivery of neural stem cells and growth factors for central nervous system repair, Acta Biomater. 9 (6) (2013) 6834–6843, https://doi.org/10.1016/j.actbio.2013.02.043.

[51] P.H. Westfall, S.S. Young, Resampling-based Multiple Testing: Examples and Methods for P-Value Adjustment, vol 279, John Wiley & Sons, 1993.

[52] D.S. Moore, S. Kirkland, The Basic Practice of Statistics, vol. 2, WH Freeman, New York, 2007.

[53] A.P. Bagre, K. Jain, N.K. Jain, Alginate coated chitosan core shell nanoparticles for oral delivery of enoxaparin: in vitro and in vivo assessment, Int. J. Pharm. 456 (1) (2013) 31–40, https://doi.org/10.1016/j.ijpharm.2013.08.037.

[54] X. Li, X. Kong, S. Shi, X. Zheng, G. Guo, Y. Wei, Z. Qian, Preparation of alginate coated chitosan microparticles for vaccine delivery, BMC Biotechnol. 8 (1) (2008) 1–11, https://doi.org/10.1186/1472-6750-8-89.

[55] S. Li, H. Zhang, K. Chen, M. Jin, S.H. Vu, S. Jung, N. He, Z. Zheng, M.S. Lee, Application of chitosan/alginate nanoparticle in oral drug delivery systems: prospects and challenges, Drug Deliv. 29 (1) (2022) 1142–1149, https://doi.org/10.1080/10717544.2022.2058646.

[56] D.R. Bhumkar, V.B. Pokharkar, Studies on effect of pH on cross-linking of chitosan with sodium tripolyphosphate: a technical note, AAPS PharmSciTech 7 (2006) E138–E143, https://doi.org/10.1208/pt070250.

[57] J.O. Akolade, H.O.B. Oloyede, M.O. Salawu, A.O. Amuzat, A.I. Ganiyu, P.C. Onyenekwe, Influence of formulation parameters on encapsulation and release characteristics of curcumin loaded in chitosan-based drug delivery carriers, J. Drug Deliv. Sci. Technol. 45 (2018) 11–19, https://doi.org/10.1016/j.jddst.2018.02.001.

[58] B.K. Heragh, H. Taherinezhad, G.R. Mahdavinia, P. Labib, S. Javanshir, P. Ghasemsolb, pH-responsive co-delivery of doxorubicin and saffron via cross-linked chitosan/laponite RD nanoparticles for enhanced-chemotherapy, Mater. Today Commun. 34 (2023) 104956, https://doi.org/10.1016/j.mtcomm.2022.104956.

[59] S. Mondal, S. Ghosh, S.P. Moulik, Stability of curcumin in different solvent and solution media: UV–visible and steady-state fluorescence spectral study, J. Photochem. Photobiol. B Biol. 158 (2016) 212–218, https://doi.org/10.1016/j.jphotobiol.2016.03.004.

[60] C. Sun, C. Xu, L. Mao, D. Wang, J. Yang, Y. Gao, Preparation, characterization and stability of curcumin-loaded zein-shellac composite colloidal particles, Food Chem. 228 (2017) 656–667, https://doi.org/10.1016/j.foodchem.2017.02.001.

[61] A. Bhattacharyya, F. Nasim, R. Mishra, R.P. Bharti, P.P. Kundu, Polyurethane-incorporated chitosan/alginate core–shell nano-particles for controlled oral insulin delivery, J. Appl. Polym. Sci. 135 (26) (2018) 46365, https://doi.org/10.1002/app.46365.

[62] J.P. Holman, Unsteady heat conduction (chapter 4). Text Book "Heat Transfer, tenth ed., McGrawHill Higher Education, 2010.

[63] H. Abdelkader, S.A. Hussain, N. Abdullah, S. Kmaruddin, Review on micro-encapsulation with Chitosan for pharmaceuticals applications, MOJ Current Research & Reviews 1 (2) (2018) 77–84, https://doi.org/10.15406/mojcrr.2018.01.00013.

[64] S. Fund, P. Sahni, P.D. Shere, D. Shere, Microencapsulation optimization and storage stability of curcumin in maltodextrin and gelatin, Journal of Hill Agriculture 9 (4) (2018) 447–451, https://doi.org/10.5958/2230-7338.2018.00061.7.

[65] W. Wang, X. Hao, S. Chen, Z. Yang, C. Wang, R. Yan, X. Zhang, H. Liu, Q. Shao, Z. Guo, pH-responsive Capsaicin@ chitosan nanocapsules for antibiofouling in marine applications, Polymer 158 (2018) 223–230, https://doi.org/10.1016/j.polymer.2018.10.067.

[66] F. Reyes-Ortega, pH-responsive polymers: properties, synthesis and applications, in: Smart Polymers and Their Applications, Woodhead Publishing, 2014, pp. 45–92, https://doi.org/10.1533/9780857097026.1.45.

[67] M. Saeedi, O. Vahidi, M.R. Moghbeli, S. Ahmadi, M. Asadnia, O. Akhavan, F. Seidi, M. Rabiee, M.R. Saeb, T.J. Webster, R.S. Varma, Customizing nano-chitosan for sustainable drug delivery, J. Contr. Release 350 (2022) 175–192, https://doi.org/10.1016/j.jconrel.2022.07.038.

[68] P.I. Lee, Kinetics of drug release from hydrogel matrices, J. Contr. Release 2 (1985) 277–288, https://doi.org/10.1016/0168-3659(85)90051-3.

[69] P.L. Ritger, N.A. Peppas, A simple equation for description of solute release I. Fickian and non-fickian release from non-swellable devices in the form of slabs, spheres, cylinders or discs, J. Contr. Release 5 (1) (1987) 23–36, https://doi.org/10.1016/0168-3659(87)90034-4.